318 *Biochemistry* **2010,** *49,* 318–328
DOI: 10.1021/bi9016389

BIOCHEMISTRY
including biophysical chemistry & molecular biology
Article

Calmodulin-Induced Conformational and Hydrodynamic Changes in the Catalytic Domain of *Bordetella pertussis* Adenylate Cyclase Toxin[†]

Johanna C. Karst,[‡] Ana Cristina Sotomayor Pérez,[‡] J. Iñaki Guijarro,[§] Bertrand Raynal,[∥] Alexandre Chenal,*[,‡,⊥] and Daniel Ladant*[,‡,⊥]

[‡]*Institut Pasteur, Unité de Biochimie des Interactions Macromoléculaires, CNRS URA 2185, Département de Biologie Structurale et Chimie, 25-28 rue du Dr. Roux, 75724 Paris Cedex 15, France,* [§]*Institut Pasteur, Unité de RMN des Biomolécules, CNRS URA 2185, Département de Biologie Structurale et Chimie, 25-28 rue du Dr. Roux, 75724 Paris Cedex 15, France, and* [∥]*Institut Pasteur, Plate-Forme de Biophysique des Macromolécules et de leurs Interactions, CNRS URA 2185, Département de Biologie Structurale et Chimie, 25-28 rue du Dr. Roux, 75724 Paris Cedex 15, France.* [⊥]*These authors contributed equally to this work.*

Received September 18, 2009; Revised Manuscript Received December 8, 2009

ABSTRACT: *Bordetella pertussis*, the causative agent of whooping cough, secretes among various toxins an adenylate cyclase (CyaA) that displays a unique mechanism of cell invasion, which involves a direct translocation of its N-terminal catalytic domain (AC, 400 residues) across the plasma membrane of the eukaryotic targeted cells. Once into the cytosol, AC is activated by endogenous calmodulin and produces toxic amounts of cAMP. The structure of AC in complex with the C-terminal part of calmodulin has recently been determined. However, as the structure of the catalytic domain in the absence of calmodulin is still lacking, the molecular basis of AC activation by calmodulin remains largely unknown. To characterize this activation mechanism, we investigated here the biophysical properties of the isolated catalytic domain in solution with or without calmodulin. We found that calmodulin triggered only minor modifications of the protein secondary and tertiary structure but had a pronounced effect on the hydrodynamic properties of AC. Indeed, while the isolated catalytic domain was spherical and hydrated, it underwent a significant elongation as well as compaction and dehydration upon calmodulin interaction. On the basis of these data, we propose a model for the structural transition between the calmodulin-free and calmodulin-bound AC.

The adenylate cyclase toxin (CyaA)[1] produced by *Bordetella pertussis*, the causative agent of whooping cough, is a key virulence factor of this bacterium (*1*, *2*). It is secreted by virulent bacteria and is able to invade eukaryotic cells where, upon activation by the endogenous calmodulin (CaM), it catalyzes unregulated synthesis of cAMP to pathogenic levels. The CyaA toxin plays an important role in the early stages of respiratory tract colonization by *B. pertussis*. Through its interaction with a cellular receptor, the CD11b/CD18 integrin, CyaA targets cells from the innate immune system (i.e., neutrophils, macrophages, etc.) and impairs their phagocytic functions (*3*−*5*). CyaA is a 1706-residue protein: the CaM-activated catalytic domain (AC) is located in the 400 amino-proximal residues, while the carboxy-terminal 1306 residues constitute the major calcium-binding region (*6*−*8*) and are responsible for binding to target cells and translocation of the N-terminal catalytic domain across the cell plasma membrane by a yet undisclosed mechanism. The AC domain interacts with high affinity (K_D < 0.1 nM) with CaM to form a complex that exhibits a very high catalytic turnover (k_{cat} = 2000−3000 s^{-1}), while the enzymatic activity of AC alone is ∼1000-fold lower.

CyaA belongs to a subclass of adenylate cyclase enzymes that comprises different toxins secreted by pathogenic bacteria (*9*, *10*). Among them, the closest relative to CyaA and most studied member of this subfamily is the Edema factor (EF) of *Bacillus anthracis*, a toxin crucial for anthrax pathogenesis. The EF toxin associated with the *B. anthracis* protective antigen (PA) uses a receptor-mediated endocytosis pathway to enter eukaryotic cells, where it is, like CyaA, activated by CaM to produce supraphysiologic levels of cAMP.

Although AC and EF exhibit an only limited degree of sequence identity (*10*), they share substantial similarity in their tertiary structures as revealed by the X-ray structures of both enzymes in complex with CaM (*10*, *11*). Most interestingly, although the respective CaM contact surfaces in the two enzymes have largely diverged, their catalytic sites, made of three highly conserved regions (CR1, residues 54−77; CR2, residues

[†]This work was supported by the Institut Pasteur, the Centre National de la Recherche Scientifique (CNRS URA 2185, Biologie Structurale et Agents Infectieux), and the European Union sixth Framework Programme contract (LSHB-CT-2004-503582) (Theravac Project). The 600 MHz NMR spectrometer was funded by the Région Ile de France and the Institut Pasteur.

*To whom correspondence should be addressed. D.L.: Unité de Biochimie des Interactions Macromoléculaires, CNRS URA 2185, Institut Pasteur, 28 rue du Dr. Roux, 75724 Paris cedex 15, France; telephone, 331 45 68 84 00; fax, 331 40 61 30 42; e-mail, daniel.ladant@pasteur.fr. A.C.: Unité de Biochimie des Interactions Macromoléculaires, CNRS URA 2185, Institut Pasteur, 28 rue du Dr. Roux, 75724 Paris cedex 15, France; telephone, 331 44 38 92 12; fax, 331 40 61 30 42; e-mail, alexandre.chenal@pasteur.fr.

[1]Abbreviations: AC, adenylate cyclase domain; CyaA, adenylate cyclase toxin; CaM, calmodulin; EF, Edema factor; HEPES, *N*-(2-hydroxyethyl)piperazine-*N*′-2-ethanesulfonic acid; λ_{max}, maximum emission wavelength; CD, circular dichroism; MRE, mean residue ellipticity; AUC, analytical ultracentrifugation; SEC-TDA, size exclusion chromatography coupled online to a triple detector array; QELS, quasi-elastic light scattering; SDS−PAGE, sodium dodecyl sulfate−polyacrylamide gel electrophoresis; R_H, hydrodynamic radius; R_0, anhydrous hydrodynamic radius; PDB, Protein Data Bank.

 Published on Web 12/09/2009

184−198; CR3, residues 295−315), are structurally identical. Prior mutagenesis studies have shown that many of the conserved residues in these segments play a direct role in the catalytic reaction (*12*−*14*). A detailed structural comparison of EF alone or as a complex with CaM revealed that one of the conserved regions (CR3) lining the active site is disordered in the absence of CaM. This study demonstrated a novel mechanism of CaM-mediated activation by active site remodeling (*15*). However, the molecular basis of CaM activation of AC remains unknown, as the structure of the isolated CyaA catalytic domain is lacking.

Prior biochemical studies have shown that the AC domain has a modular structure: it consists of two regions, T25 (residues 1−224 of CyaA) and T18 (residues 225−384) that can be obtained *in vitro* by limited proteolysis (*16*). The isolated T25 and T18 fragments can reassociate with CaM into a fully active ternary complex (*17*, *18*). The crystal structure of the CyaA catalytic domain bound to the C-terminal domain of CaM ($CaM_{C\text{-}ter}$) showed that the complex has an elongated shape and that $CaM_{C\text{-}ter}$ interacts predominantly with the C-terminal, T18 moiety of AC (*11*, *16*, *19*, *20*). In particular, an amphiphilic helical structure (residues 234−254), defined as helix H by Guo et al. (*11*), was found to be a major determinant of CaM binding.

Here, in an attempt to understand how CaM might activate CyaA, we have characterized by complementary biophysical approaches, the conformational and hydrodynamic changes of AC induced by CaM binding. We found that CaM binding triggered only limited modifications of the secondary and tertiary structures of AC but induced drastic changes in its hydrodynamic properties: while the isolated catalytic domain was spherical and hydrated, CaM interaction elicited significant elongation and dehydration of the complex. The implications of these findings for the mechanism of AC activation by CaM are discussed.

EXPERIMENTAL PROCEDURES

Materials. Hepes-d_{18} (D18, 98%, DLM-3786-0) was purchased from Cambridge Isotope Laboratories. D_2O (D215B), NaOD, and DCl were from Euriso-top (CEA Saclay, Gif-Sur-Yvette, France). All experiments were conducted in 20 mM Hepes and 150 mM NaCl (pH 7.4) (buffer A) with or without 0.2 mM $CaCl_2$ at 25 °C. The peptide $P_{233-254}$ was synthesized and purified by Genosphere Biotechnologies (Paris, France). Its sequence is LDRERIDLLWKIARAGARSAVG and corresponds to the amino acid sequence between residues 233 and 254 (native numbering) of CyaA. The peptide contains 22 amino acids and one native tryptophan and is N-acetylated. It was purified to homogeneity by reversed-phase HPLC on a C8 column using an acetonitrile/trifluoroacetic acid gradient. Its quality was assessed by matrix-assisted laser desorption ionization time of flight (MALDI-TOF). Its molecular mass determined by MALDI-TOF is 2509 Da, and its pI is computed to be 10.7.

Protein Preparation. The adenylate cyclase catalytic domain (AC) studied here corresponds to residues 1−384 of *B. pertussis* CyaA followed by a glycine and a lysine (*21*). AC was overproduced in *Escherichia coli* and purified by two sequential chromatographic steps on DEAE-Sepharose as described by Vougier et al. (*21*). The elution buffer of DEAE-Sepharose consisted of 20 mM Hepes and 500 mM NaCl (pH 7.4). AC was further purified on a Sephacryl S300 column equilibrated with buffer A. Purified AC was equilibrated in buffer A or in 20 mM NH_4HCO_3 by chromatography on prepacked G25SF desalting columns prior to lyophilization. The protein, in solution or lyophilized, was stored at −20 °C. We checked by CD and fluorescence that the lyophilization process did not affect the behavior of AC. Protein batches were homogeneous as analyzed by SDS−PAGE and N-terminal sequencing. The integrity and identity of the samples were confirmed by the measurement of the absolute molecular mass by surface-enhanced laser desorption ionization time-of-flight mass spectrometry (SELDI-TOF-MS, model PCS 4000, Ciphergen). The mass spectrum showed a single peak of 41580 ± 300 g/mol, which corresponded to the expected molecular weight (41588). A molar ε of 28880 M^{-1} cm^{-1} and a pI of 6.3 were computed from the sequence of AC.

The thermodynamic stability of AC was investigated by tryptophan fluorescence and circular dichroism. The data showed that AC was weakly stable (half-melting temperature of 41 °C) and prone to aggregation in a temperature-dependent manner. We also determined that fluorescence, far-UV, and near-UV CD spectra of AC were not sensitive to calcium (from 0 to 2 mM $CaCl_2$). We thus chose to perform all experiments at 25 °C in the presence of 0.2 mM calcium (required for full saturation of CaM).

The purified AC protein exhibited a specific enzymatic activity of 2−4 units/mg in the absence of calmodulin (CaM) and ~2000 units/mg in the presence of 2 nM CaM; it was half-maximally activated by a CaM concentration of ~0.1 nM. One unit of AC enzymatic activity, measured as described previously (*16*), corresponds to 1 μmol of cAMP formed per minute at 30 °C and pH 8.

CaM was overproduced in *E. coli* and purified as described by Vougier et al. (*21*). The first step of ammonium sulfate precipitation followed by a glacial acetic acid precipitation and a phenyl-Sepharose chromatography led to a protein, which was more than 95% pure as judged by SDS−PAGE. As performed for AC, N-terminal sequencing and mass spectrometry confirmed the integrity and identity of CaM. The mass spectrum showed a single peak of 16710 ± 100 g/mol, which was in agreement with the expected molecular weight (16709 after removal of the N-terminal methionine). A molar ε of 2980 M^{-1} cm^{-1} and a pI of 4.1 were computed from the sequence of CaM.

Circular Dichroism Spectroscopy. CD spectra were recorded on an Aviv model 215 circular dichroism spectrometer, equipped with a water-cooled Peltier unit. CD measurements were taken at a scan rate of 0.5 nm/s (step of 0.5 nm and integration time of 1 s) with a time constant of 100 ms and a bandwidth of 1 nm. Each far-UV and near-UV CD spectrum represents the average of at least five scans. Buffer A supplemented with 0.2 mM calcium was used as blank in the far-UV and near-UV regions, and these spectra were subtracted from all recorded CD spectra.

Far-UV CD spectra were recorded in rectangular quartz Suprasil cells with path lengths of 0.1 mm (106.QS, Hellma) with 25 μM protein (AC, CaM, the AC−CaM complex, or a 1:1 peptide/CaM mixture) or 90 μM for the free peptide in buffer A supplemented with 0.2 mM $CaCl_2$. The CD unit used is the mean residue ellipticity $[\theta]_F$ (MRE) expressed in degrees square centimeter per decimole residue ($deg \cdot cm^2 \cdot dmol^{-1} \cdot res^{-1}$) and calculated as previously described (*8*).

Measured ellipticity in millidegrees obtained for individual AC (386 residues) and CaM (148 residues) spectra were added and converted to mean residue ellipticity taking into account the total number of residues present in a complex in a 1:1 stoichiometry, i.e., 534 residues. The resulting spectrum was compared to the

spectrum of the AC−CaM sample. A similar analysis was performed with peptide $P_{233-254}$ (22 residues).

Near-UV CD measurements were taken by using a tandem cuvette (238.QS, Hellma). Proteins were placed in separated chambers and then mixed in the same cuvette without removing the sample, thereby maintaining identical contents before and after mixing. AC at 30 μM (or peptide at 45 μM) and CaM at 30 μM in buffer A supplemented with 0.2 mM $CaCl_2$ were placed into separate chambers of the tandem cuvette, and spectra were recorded at 25 °C. Proteins in the two chambers were then mixed by inversion of the cuvette, and spectra were recorded under the conditions described above. The CD unit used is the molar ellipticity $[\theta]_N$, expressed in degrees square centimeter per decimole (deg cm^2 $dmol^{-1}$) and calculated as previously described (*8*).

Spectra in the far-UV region were deconvoluted using five algorithms (*22*−*24*) available at the DICHROWEB server: Contin-LL, Selcon 3, CDSSTR, VARSLC, and K2d. Here, only the results obtained with the CDSSTR program from W. C. Johnson (*25*−*27*) are reported as they provided the best fits to all data.

Fluorescence Spectroscopy. Measurements were performed with an FP-6200 spectrofluorimeter (Jasco) in a Peltier-thermostated cell holder, using a 1 cm path length quartz cell (101.QS, Hellma). A bandwidth of 5 nm was used for the excitation and emission beams. The peptide concentration was 1 μM in buffer A supplemented with 0.2 mM $CaCl_2$. Calmodulin was progressively added in the cuvette that contained the peptide (at final concentrations ranging from 0 to 10 μM). For tryptophan intrinsic fluorescence, the excitation wavelength was fixed at 290 nm. The emission spectra were recorded at 25 °C, from 300 to 400 nm at a scan rate of 125 nm/min. The maximum emission wavelength (λ_{max}) and fluorescence intensity ratio at 360 nm to 320 nm (FIR 360/320) represent the average of three values obtained from emission spectra that were corrected for blank measurements.

Nuclear Magnetic Resonance Spectroscopy (*NMR*). NMR experiments were conducted on an Inova (Varian Inc., Palo Alto, CA) spectrometer with a 14.7 T magnetic field (600 MHz proton resonance frequency) equipped with a cryoprobe. VnmrJ version 2.1B (Varian) was used to record and process data. Proteins were desalted against 10 mM NH_4HCO_3 on G25SF and then lyophilized. Buffer A prepared with deuterated Hepes (d18, Cambridge Isotope Laboratories) and D_2O (99.99%) was lyophilized twice and resuspended in D_2O to remove residual H_2O. The lyophilized proteins were resuspended in a given volume of this buffer, incubated for 1 h at room temperature to exchange amide protons, and freeze-dried. Proteins were then resuspended in the same volume of D_2O used prior to lyophilization. One-dimensional (1D) ^1H spectra were recorded at 25 °C with AC (40 μM), CAM (50 μM), and a 1:1 AC−CaM mixture (30 μM) in deuterated buffer A. The buffer was supplemented with 2 mM $CaCl_2$ for AC and AC−CaM samples. Sixty-four transients with a spectral width of 12 ppm were accumulated. The water signal was suppressed by very low power irradiation (0.5 s) during the 2 s recovery delay.

Saturation transfer experiments between aromatic and aliphatic protons were performed by selectively saturating a bandwidth of 1.5 ppm of the aromatic region centered at 7.2 ppm in the saturation experiment or off resonance at 15 ppm in the reference experiment. Selective saturation was achieved using trains of 90° Gaussian pulses. Experiments were conducted with 24 accumulations for each saturation time that varied between 0 and 2.2 s. The transferred saturation or NOE (nuclear Overhauser enhancement) was calculated using the formula $NOE = |(I_S - I_R)/I_R|$, where I_S and I_R represent the intensities of the aliphatic region (upfield of 1.1 ppm) of the on and off resonance experiments, respectively. Buildup curves (NOE vs saturation time t) were fit using an isolated spin-pair relaxation model {$NOE = \sigma/\rho[1 - \exp(-\rho t)]$, where σ (s^{-1}) represents the cross-relaxation rate and ρ (s^{-1}) the autorelaxation rate}.

Analytical Ultracentrifugation. Sedimentation equilibrium and velocity experiments were performed on a ProteomeLab XL-I analytical ultracentrifuge (Beckman Coulter) in an AN60-Ti rotor at 25 °C. The samples were filtered on 0.2 μm filters before the experiments. Detection of the protein concentration as a function of radial position and time was performed by optical density measurements at a wavelength of 276 or 230 nm. The buffer was buffer A supplemented with 0.2 mM $CaCl_2$. The computed viscosity η and density ρ of this buffer were (SEDNTERP version 1.09) 0.908 cP and 1.004 g/mL at 25 °C, respectively. For sedimentation equilibrium experiments, the CaM sample (120 μL, 50 μM) was loaded in a 1.2 mm thick two-channel Epon centerpiece. It was centrifuged for 24 h at a rotor speed of 25000 rpm, then for 15 h at 30000 rpm, and finally for 10 h at 35000 rpm. The AC sample (40 μL, 19 μM) was loaded in a 1.2 mm thick six-channel Epon centerpiece and was then centrifuged for 3 h at a rotor speed of 12000 rpm, for 2 h at 15000 rpm, and for 2 h at 18000 rpm. Finally, the AC−CaM complex sample (150 μL, 17 μM for both proteins) was loaded in a 1.2 mm thick two-channel aluminum centerpiece. The complex was centrifuged for 10 h at a rotor speed of 12000 rpm, then for 7 h at 15000 rpm, and finally for 7 h at 18000 rpm. Data were recorded for each speed after it had been determined that sedimentation−diffusion equilibrium had been effectively reached. Baseline was measured at 42000 rpm after 2 h for CaM and 50000 rpm for AC and the complex. Radial distributions were analyzed by global fitting of the three speeds using the one-species model in Ultrascan version 9.5 (*28*). The partial specific volume was obtained by fixing the molecular mass to the mass of the monomer determined by mass spectrometry.

For sedimentation velocity experiments, the protein samples (400 μL, 17 μM) were loaded in a 1.2 mm thick two-channel aluminum centerpiece and spun at 60000 rpm for CaM or 50000 rpm for AC and the complex. Data were analyzed with Sedfit version 11.3 (*29*) using a continuous size distribution [$c(s)$] model with a level of confidence of 0.95. Monte Carlo analysis (1000 iterations) were conducted for each plot with Sedfit (*30*). The errors were below 0.05%, showing the robustness of the fits. The three species, AC, CaM, and the AC−CaM complex, were analyzed by sedimentation velocity experiments at three additional concentrations (8, 14, and 27 μM), yielding similar profiles. The hydrodynamic radius, R_H, was calculated using the sedimentation coefficient value and the molecular mass determined by size exclusion chromatography coupled online to TDA.

Size Exclusion Chromatography Coupled Online to Hydrodynamic Measurements. Size exclusion chromatography (SEC) was carried out on a Superdex 200 column (GE Healthcare). It was controlled by a GPCmax module connected online to a model 302 triple detector array (TDA) (Viscotek Ltd., Houston, Basingstoke, U.K.). The oven of the TDA contained (i) a static light scattering cell with two photodiode detectors, at 7° for low-angle (LALS) and at 90° for right-angle laser light scattering (RALS), (ii) a deflection refractometer, (iii) a photometer, and (iv) a differential viscometer. The general procedures

have been described previously (*8*). Briefly, all solutions were filtered on 0.2 μm filters and allowed to equilibrate at 25 °C prior to being run. Buffer A supplemented with 0.2 mM $CaCl_2$ was used, and the SEC experiments were performed at 22 °C. The detections in the TDA oven were conducted at 25 °C. All experimental sequences contained injections of BSA used for TDA calibration (2 mg/mL, various volumes) and at least four injections of different volumes of the tested protein (i.e., 20 μM AC, 40 μM CaM, and 17 μM AC−17 μM CaM complex). The refractive index increments, dn/dc, were experimentally determined. All data were acquired and processed using Omnisec (Viscotek Ltd.). Protein concentrations were determined using both the photometer and the deflection refractometer. The RALS and LALS data coupled to the concentration provided the molecular mass. Finally, the differential viscometer measurements, in conjunction with concentration, provided the intrinsic viscosity.

Protein Shape and Hydration. The viscosity increment ν (the Simha−Einstein hydrodynamic function related to the axial ratio a/b) of proteins can be calculated by inverting Einstein's viscosity relation: $M[\eta] = \nu V_H N_A$ to $\nu = M[\eta]/(V_H N_A)$, where V_H is the hydrodynamic volume defined by $V_H = 4\pi R_H^3/3$, $[\eta]$ is the intrinsic viscosity, and N_A is Avogadro's number. The R_H values are calculated from the sedimentation coefficient and molecular mass (see above). Hydration δ_{IV} is calculated from the intrinsic viscosity measurement. The intrinsic viscosity in a defined solvent depends on the shape, the molecular volume of the protein, and electroviscous effects. Its expression is the product of the hydrodynamic function ν and the swollen volume V_s according to $[\eta] = \nu V_s = \nu(\bar{\nu} + \delta_{IV}/\rho)$, where the swollen volume is given by the sum of the partial specific volume $\bar{\nu}$ of the protein (volume occupied by 1 g of protein) and the hydration of the protein (mass of water per mass of protein in grams per gram). The hydration parameter δ_{IV} of the protein, which can be extracted from the latter relation $\delta_{IV} = ([\eta]/\nu - \bar{\nu})\rho$, includes (i) the water molecules bound to the protein and (ii) the water molecules dragged by the diffusion of the protein and/or influenced by being in the vicinity of the protein. The molecular mass M was measured by static light scattering, the partial specific volume $\bar{\nu}$ by equilibrium AUC, and the R_H by velocity AUC (see above). The viscosity increment provides the axial ratio a/b of the semi axes a and b (with $a > b$) that describe the shape of an ellipsoid of revolution. All theses procedures are described elsewhere (*8*, *31*).

RESULTS

Conformational Studies of AC and CaM in Solution Followed by Circular Dichroism and Fluorescence Spectroscopies. Modifications of the secondary and tertiary structure contents of the AC polypeptide upon CaM binding were characterized by circular dichroism (CD) spectroscopy. The far-UV CD spectrum of CaM was characteristic of an α-helical protein with minima at 208 and 222 nm (Figure 1A). The secondary structure content was estimated by deconvolution procedures using DICHROWEB (*22*−*27*) (see Experimental Procedures and Table 1). The secondary structure content was in good agreement with that deduced from the NMR solution structure of calmodulin (*32*). The far-UV CD spectrum of AC appeared rather unusual with a positive π_0−π^* band around 190 nm, a negative π_0−π^* band at 207 nm, and a weak negative n′−π^* band, appearing as a shoulder around 220 nm

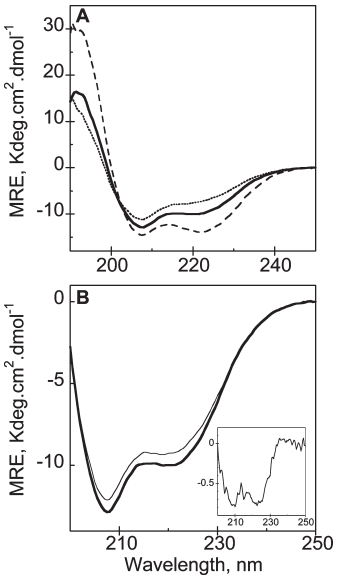

FIGURE 1: Far-UV CD spectra of AC, CaM, and the AC−CaM complex. (A) Far-UV CD spectra of AC [25 μM (···)], CaM [25 μM (---)], and the AC−CaM complex [25 μM for both proteins (—)]. (B) Sum of the spectra of the two isolated components (thin line) for comparison with the AC−CaM experimental spectrum (thick line). The inset shows the calculated difference between the spectrum of the mixture of the two components and the sum of the spectra of the unmixed components. Experimental conditions: buffer A at 25 °C supplemented with 0.2 mM $CaCl_2$.

Table 1: Secondary Structure of CaM, AC, and the AC−CaM Complex[a]

	CaM[b]	AC[b]	AC−CaM[b]	AC + CaM[c]
α-helix	50	24	35	31
β-sheet	14	19	13	18
turns	14	17	18	16
random coil	21	40	34	35
root-mean-square error	0.012	0.022	0.034	

[a]Deconvolution of the far-UV CD spectra was performed using DICHROWEB (*23*). The deconvolution results shown here are those provided by CDSSTR. [b]From experimental data [c]Theoretical sum of the spectra of AC and CaM

(Figure 1A). The band located at 207 nm may be assigned to a combination of the negative π_0−π^* band of an extended conformation arising at 200 nm and the negative contribution of the exciton splitting of the π_0−π^* band of α-helices at 210 nm. The secondary structure content of AC deduced from this CD spectrum was estimated to be ≈24% α-helices and ≈19% β-sheets (Table 1). The spectrum of the AC−CaM complex at an equimolar ratio was quite similar (Figure 1A), also displaying a negative π_0−π^* band around 207 nm and a negative n′−π^* band around 220 nm. Upon deconvolution of this CD spectrum, the overall secondary structure composition of the AC−CaM complex [≈35% α-helices and ≈13% β-sheets (Table 1)] turned out to be significantly different from that deduced from the X-ray structure of the AC−$CaM_{C\text{-}ter}$ complex which showed a higher proportion of helical structures (≈45% according to PDB entry 1YRU) (*11*). Although secondary structure predictions from CD spectra may sometimes be relatively inaccurate, the variation in α-helical content found could also result from the differences in the AC and CaM polypeptides examined in each case: our AC protein encompasses residues 1−386 and a full-length CaM

molecule, while the X-ray structure was determined with a crystal made of a complex of AC residues 1−364 bound to only the C-terminal half of CaM (*11*). Finally, aromatic residues of AC might also affect the far-UV CD spectrum, thus altering the secondary structure content deconvolution (*33*−*35*). It should be stressed that the AC−CaM complex characterized here was fully functional from an enzymatic point of view, exhibiting a high catalytic turnover (k_{cat} = 2000−3000 s^{-1}) and behaved as a homogeneous species according to its hydrodynamic properties (see below). Thus, the CD spectral properties reported here likely reflect the intrinsic structural characteristics of the active AC−CaM complex in solution.

To characterize the conformational changes that resulted from binding of CaM to AC, we compared the experimental spectrum of the AC−CaM complex (Figure 1B, thick line) with the sum (thin line) of the spectra of the two individual proteins at equimolar concentrations (see Experimental Procedures). As shown in Figure 1B, the spectra revealed a significant increase in absolute values in the ellipticity of the AC−CaM complex as compared to that of the two separated proteins. Interestingly, the difference spectrum [i.e., AC−CaM − (AC + CaM), at equimolar concentrations], as shown in the inset of Figure 1B, displayed two major bands at 223 and 208 nm, suggesting that the formation of the AC−CaM complex is accompanied by an increase in the α-helical content of the polypeptides. Assuming that a signal of −30 K deg·cm^2·$dmol^{-1}$ at 223 nm corresponds to ≈100% α-helical content (*36*), the variation of the ellipticity of approximately −1.1 ± 0.3 K deg·cm^2·$dmol^{-1}$ should correspond to an increment of ∼3.7 ± 1% in α-helical content. This corresponds to ∼20 ± 5 amino acids of a total of 534 residues (386 AC residues plus 148 CaM residues) acquiring an α-helical structure upon interaction of the two polypeptides. It is likely that this increase in α-helical content involved mainly the AC polypeptide, as it has been previously reported that the secondary structure content of CaM (and, hence, its far-UV CD spectrum) was not significantly affected by its binding to its targets (*37*−*39*). However, the possibility that secondary structural changes also occurred in CaM upon binding to AC cannot be excluded.

Previous biochemical and structural studies have shown that the sequence located around tryptophan 242 (W242) represents a major CaM binding determinant of AC, and that it adopts an amphiphilic helical structure [H helix according to Guo et al. (*11*)] typical of many CaM-binding sites. We hypothesized that this segment might undergo a transition from random coil to helix upon association with CaM. We examined therefore potential CaM-induced conformational changes in a synthetic peptide of 22 amino acid residues ($P_{233-254}$) corresponding to the H helix sequence (from residue L233 to G254 in the native numbering of CyaA). The intrinsic fluorescence of the single tryptophan residue W242 was used to demonstrate that peptide $P_{233-254}$ bound to CaM (which has no tryptophan residue) in a calcium-dependent manner, in agreement with previous results (*17*). While the free peptide exhibited a maximum emission wavelength (λ_{max}) at 357 nm, the addition of saturating amounts of CaM resulted in a blue shift (λ_{max} = 340 nm) and an increase in the fluorescence intensity (inset of Figure 2A), suggesting that the W242 moved from a solvent-exposed environment toward a more apolar one. The increase in fluorescence emission at 320 nm was used to monitor binding of peptide $P_{233-254}$ to CaM. These titration experiments (Figure 2A) indicated that at CaM of concentrations of >1 μM, the peptide (1 μM) was almost totally bound to CaM. The CaM−peptide interaction was then examined by CD spectroscopy. The far-UV CD spectrum of the free peptide showed a strong negative band at 202 nm, characteristic of extended conformations, while the spectrum of the CaM−peptide complex at the same concentration (10 μM) revealed a high helical content (Figure 2B). The difference spectrum corresponding to the experimental spectrum of the $P_{233-254}$−CaM complex minus the sum of the individual $P_{233-254}$ and CaM spectra clearly showed a gain in α-helix content (inset of Figure 2B) upon association. Hence, these data suggest that upon binding to CaM, the $P_{233-254}$ peptide undergoes a transition from a random coil toward a helix-rich conformation.

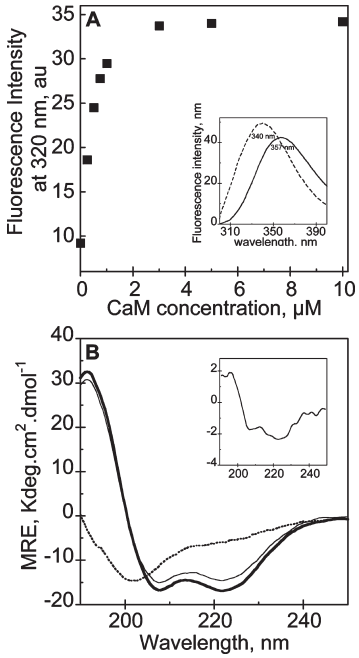

FIGURE 2: Fluorescence and far-UV CD spectra of peptide $P_{233-254}$ in the presence and absence of CaM. (A) Fluorescence intensity at 320 nm (excitation at 290 nm) of 1 μM peptide $P_{233-254}$ in the presence of increasing amounts of CaM (from 0 to 10 μM). Spectra were averaged (three replicates), and the contribution of the buffer was subtracted. The inset shows tryptophan intrinsic fluorescence spectra of peptide $P_{233-254}$ (1 μM) in the absence (—) or presence of CaM (---). (B) Far-UV CD spectra of the free peptide $P_{233-254}$ [90 μM (···)] and the $P_{233-254}$−CaM complex [both components at 25 μM (thick line)]. The sum of the spectra of the two isolated components (at the same concentration of 25 μM) is also reported for comparison (thin line). The inset shows the calculated difference between the spectrum of the mixture of the two components and the sum of the spectra of the unmixed components. In panel B, scales have been adjusted to show the difference between spectra. Experimental conditions: buffer A with 0.2 mM $CaCl_2$ at 25 °C.

Near-UV CD spectroscopy was used to characterize the tertiary structure content of AC, CaM, and the AC−CaM complex (Figure 3A,B). The near-UV CD spectrum of CaM showed two relatively intense negative peaks near 262 and 268 nm arising from phenylalanine residues and a weak negative signal from 270 to 290 nm from tyrosine residues (Figure 3A). The near-UV CD spectrum of AC exhibited a large negative band encompassing the aromatic region (Figure 3A). The two negative peaks at 262 and 269 nm could be assigned to phenylalanine residues, whereas the strong negative band between 270 and 280 nm arose from tyrosine and/or tryptophan residues constrained in chiral environments. It is noteworthy that the L_b band of the two tryptophans of AC did not show any chiral activity around 292 nm.

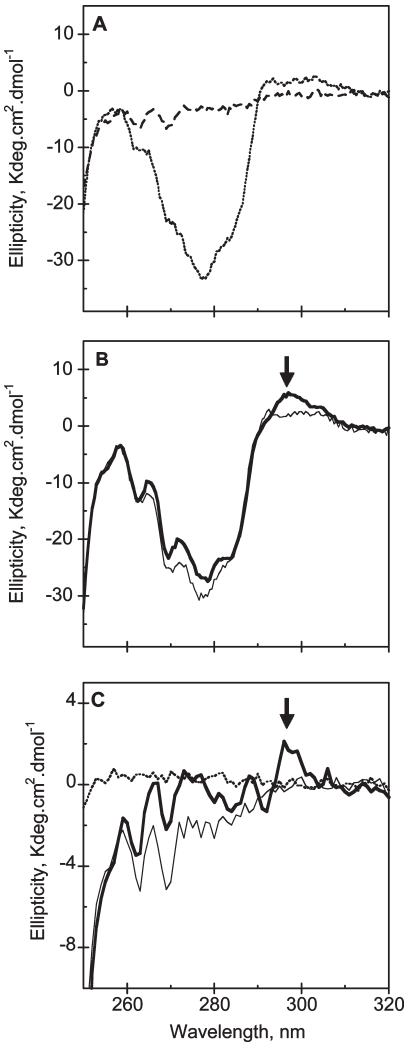

FIGURE 3: Near-UV CD spectra of AC, CaM, and the AC−CaM complex, as well as of peptide $P_{233-254}$ and of the peptide−CaM complex. (A) Near-UV CD spectra of AC [30 μM (···)] and CaM [30 μM (---)]. (B) Near-UV CD spectra of AC and CaM (30 μM each protein) either separated (thin line) or mixed (thick line) in a tandem cuvette. (C) Near-UV CD spectra of free peptide $P_{233-254}$ [45 μM (···)] and of $P_{233-254}$ and CaM (45 and 30 μM, respectively) either separated (thin line) or mixed (thick line) in a tandem cuvette. The arrows highlight the region of the tryptophan L_b band. Experimental conditions: buffer A with 0.2 mM $CaCl_2$ at 25 °C.

To monitor precisely the changes induced upon association of AC with CaM, we used a tandem cuvette in which the two proteins were placed into separated chambers. A spectrum of the separated proteins was first recorded (Figure 3B), and then the two proteins were mixed (by inverting the cuvette) before a spectrum of the complex was recorded. As shown in Figure 3B, a slight increase in the magnitude of the dichroic signal from 270 to 285 nm and a significant change around 290 nm were observed as a result of the interaction between the two proteins. The ellipticity of AC dominates the near-UV CD spectrum because CaM had only minor contributions in this spectral region. Importantly, the appearance of a positive L_b band at 295 nm in the mixed sample could be assigned to the immobilization of the tryptophan residues of AC upon formation of the AC−CaM complex.

The association between CaM and the $P_{233-254}$ peptide was also examined by near-UV CD. As shown in Figure 3C, the free peptide exhibited negligible CD intensities in the near-UV range, as expected for a flexible peptide with its unique aromatic residue

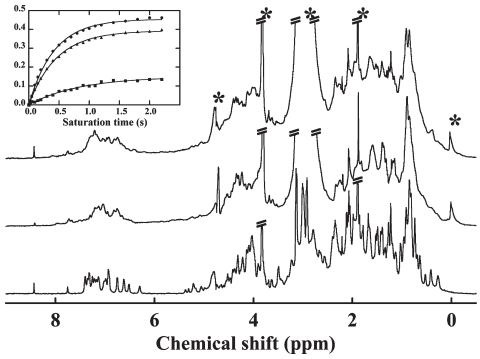

FIGURE 4: NMR one-dimensional proton spectra of CAM (bottom), AC (middle), and a 1:1 AC−CAM mixture (top) recorded at 25 °C in deuterated buffer A. The peaks belonging to residual water and the buffer are denoted with an asterisk. The inset shows the results of saturation transfer experiments. The intensity of the NOE between aromatic and aliphatic protons as a function of the saturation time is displayed. The solid line corresponds to the fit of the NOE data to an isolated spin-pair model as indicated in Experimental Procedures.

(W242) exposed to the solvent. CaM and the peptide were then loaded separately in the tandem cuvette, and near-UV CD spectra were recorded before and after mixing. The spectrum of peptide and CaM, in separated compartments of the tandem cuvette, was similar to that of CaM alone (Figure 3C), whereas when both proteins were mixed, a positive band appeared in the tryptophan L_b region (Figure 3C). It is noteworthy that this band was very similar to that observed in the spectrum of the AC−CaM complex, suggesting that the dichroic signal at 295 nm arose mainly from the W242 residue of AC.

Altogether, the CD data suggest that the sequence situated around W242 may adopt an extended conformation in the isolated catalytic domain. CaM binding could then induce the formation of an α-helix in this region of AC and constrain residue W242 in a chiral environment.

Conformational Studies of AC in Solution Followed by NMR Spectroscopy. The 1D spectrum of CaM (Figure 4) was characteristic of a structured protein with secondary and tertiary structures: it showed very good dispersion of signals in the aromatic (6−8 ppm) and aliphatic (0−6 ppm) regions, as well as upfield-shifted signals in the methyl region (≤0.8 ppm). The existence of some downfield-shifted signals in the Hα region (≥5.0 ppm) indicated that the protein contained few residues implicated in β-sheet structures. Conversely, the existence of many upfield-shifted signals with respect to their corresponding random coil values showed that the protein was rich in α-helical structures. The 1D spectrum of AC also showed well-spread resonances revealing that the protein was folded (Figure 4). Compared to the spectrum of CaM (17 kDa), the spectrum of AC (42 kDa) exhibited very broad lines as would be expected for a compact protein larger in size. The line width, which depends on the tumbling rate of a molecule and on its internal dynamics, seemed rather homogeneous in each region of the spectrum, which suggested that AC did not present large disordered regions. The Hα region of the AC spectrum showed many downfield-shifted and upfield-shifted resonances relative to their random coil values, indicative of extensive β-sheet and α-helical structures, respectively.

The spectrum of the 1:1 (molar ratio) AC−CaM mixture showed broader lines than the AC or CaM spectra, which indicated that the proteins giving rise to these signals had higher molecular weights than AC and CaM, and hence that a complex

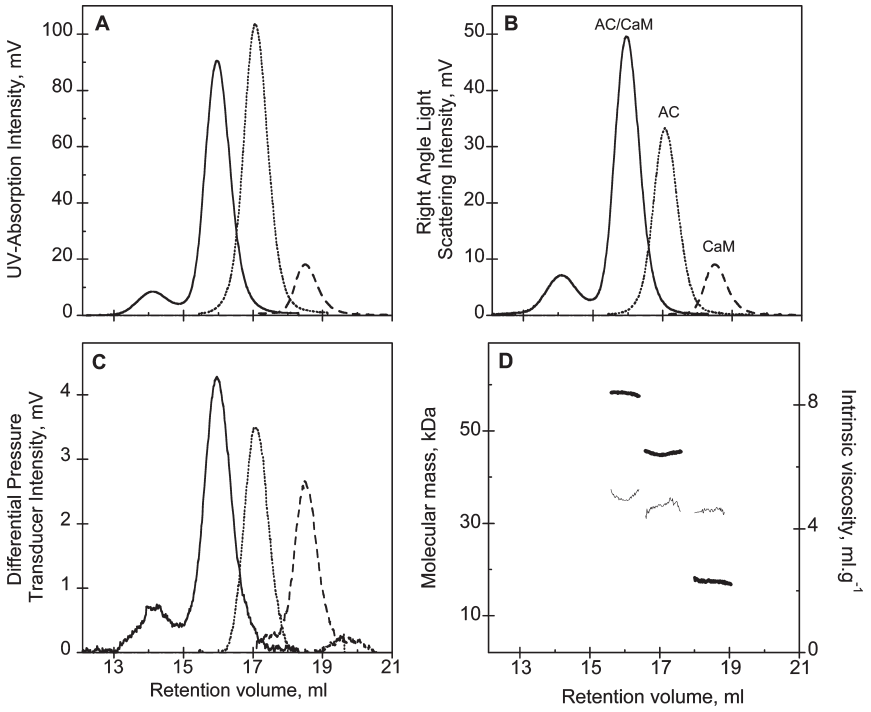

FIGURE 5: Size exclusion chromatography as followed by a triple detector array (Viscotek) of AC (···), CaM (---), and the AC−CaM complex (—): (A) UV absorption chromatogram, (B) right angle light scattering chromatogram, (C) differential pressure chromatogram, and (D) molecular mass (left *y* axis, thick line) and intrinsic viscosity (right *y* axis, thin line) for each species. Experimental conditions: buffer A with 0.2 mM $CaCl_2$ at 25 °C.

was formed. Using apodization functions for Fourier transform to preferentially observe slowly relaxing signals (narrow lines), we could not detect the spectrum of free CaM. Hence, no significant amount of free CaM was present in the complex mixture, which indicated that the stoichiometry of the interaction was 1:1.

The compactness of AC, CaM, and the AC−CaM complex was further analyzed using saturation transfer experiments (inset of Figure 4). The aromatic region of the 1D spectrum of each sample was saturated by a train of selective 90° pulses, and the intensity of the methyl region was followed as a function of the saturation time. The high values of the steady state NOE or transferred saturation (plateau value) obtained for CaM, AC, and the AC−CaM complex indicated that the aromatic residues were in close contact with aliphatic protons, and hence that the probed molecular species were compact. The magnitude of the steady state NOE depends not only on the density of the proton network (compactness) but also on the tumbling rate of a molecule and hence its size. Thus, the fact that the AC−CaM (0.45 ± 0.01) mixture showed a higher steady state NOE than AC (0.39 ± 0.01) and CaM (0.16 ± 0.01) also indicated that the complex was formed.

Hydrodynamic Properties of the AC−CaM Complex in Solution. The hydrodynamic properties (sedimentation coefficient, partial specific volume, molecular mass, hydrodynamic radius, shape, and hydration) of AC, CaM, and AC−CaM samples were analyzed by combining analytical ultracentrifugation (AUC) and size exclusion chromatography coupled online to a triple detector array (SEC-TDA). As shown in Figure 5 and Table 2, the molecular masses of AC and CaM determined by SEC-TDA (43.8 ± 0.2 kDa for AC and 17.2 ± 0.2 kDa for CaM) corresponded to those expected for the monomeric state of these proteins. The pressure imbalances generated by both proteins and measured by the differential pressure transducers (Figure 5C) allowed calculation of an intrinsic viscosity of 5.2 ± 0.1 mL/g for AC and 4.9 ± 0.1 mL/g for CaM (Table 2).

The AC−CaM sample was eluted as a major peak (> 90% of the total intensity) with a molecular mass expected for the AC−CaM complex in a 1:1 stoichiometry (Figure 5 and Table 2). An intrinsic viscosity of 5 ± 0.1 mL/g was calculated for this AC−CaM complex. A minor peak eluting at a retention volume of 14 mL was detected, but the amount was too small to accurately determine the hydrodynamic properties of the species giving rise to this peak. Additional hydrodynamic parameters, listed in Table 2, were determined by analytical ultracentrifugation (AUC) (Figure 6). In agreement with SEC-TDA, a small amount (< 15%) of a higher-molecular mass species was observed in the AC−CaM sample in sedimentation velocity experiments (this species was detected only upon data analysis with a low level of confidence, 0.55 instead of 0.95, and because of its low abundance, it could not be further characterized). From the sedimentation coefficient (*S*), we determined hydrodynamic radii (R_H) of 2.3 ± 0.1 nm for CaM, 3.3 ± 0.3 nm for AC, and 3.3 ± 0.3 nm for the complex. These values indicated that a strong compaction occurred upon formation of the complex as a R_H of at least 3.7 nm would be expected upon addition of the hydrodynamic volumes of the separated proteins. It is noteworthy that quasi-elastic light scattering (QELS) analysis of the same samples gave very similar R_H values (data not shown).

From the hydrodynamic parameters measured by TDA and AUC, we ascribed the respective contributions of hydration and shape factor to the intrinsic viscosity values (*8*). We first extracted the viscosity increment (ν) of the three studied species (see Table 2 and Experimental Procedures for details). The viscosity increment is a hydrodynamic function related to the axial ratio (a/b) of the semi-axes *a* and *b* of an ellipsoid of revolution (*40*). The viscosity increment of CaM corresponded to that of an elongated

Table 2: Hydrodynamic Parameters of CaM, AC, and the AC−CaM Complex

	CaM	AC	AC−CaM
retention volume[a] (mL)	18.5 ± 0.1	17.2 ± 0.1	16.0 ± 0.1
molecular mass[a] (kDa)	17.3 ± 0.2	43.8 ± 0.2	58.4 ± 0.2
intrinsic viscosity[a] (mL/g)	4.9 ± 0.1	5.2 ± 0.1	5.0 ± 0.1
partial specific volume[b] $\bar{\nu}$ (mL/g)	0.740 ± 0.001	0.736 ± 0.001	0.745 ± 0.001
sedimentation coefficient[b] (S)	2.0 ± 0.1	3.3 ± 0.2	4.4 ± 0.4
R_0 anhydrous[c] (nm)	1.7	2.3	2.6
R_H[b] (nm)	2.3 ± 0.1	3.3 ± 0.3	3.3 ± 0.3
frictional ratio[b] (f/f_o)	1.32 ± 0.07	1.44 ± 0.09	1.26 ± 0.11
viscosity increment[d]	2.9 ± 0.2	2.4 ± 0.2	3.4 ± 0.3
a/b[e]	2.0 ± 0.4	1	2.7 ± 0.3
hydration[d] δ_{IV} (g/g)	1.0 ± 0.1	1.5 ± 0.1	0.7 ± 0.1
computed hydration (g/g)[f]	0.48	0.41	0.43

[a]Experimental data from TDA. [b]Experimental data from AUC. [c]Hydrodynamic radius of an anhydrous and spherical molecule with equivalent M and $\bar{\nu}$. [d]The viscosity increment and hydration were calculated as described in Experimental Procedures. [e]Assuming a prolate shape. [f]Computed using SEDNTERP.

shape ($a/b \approx 2$), in good agreement with the known three-dimensional structure that consists of two globular domains connected by an elongated and flexible linker (*32*). In contrast, the isolated AC domain exhibited a viscosity increment of 2.5 that corresponds to an a/b axial ratio of 1 ($a = b = R_H$) (*40*). This result suggests that AC adopted a spherical conformation. Interestingly, the value of the viscosity increment of the AC−CaM complex indicated that its shape diverged significantly from that of a sphere. Indeed, with an axial ratio of ~2.7 (Table 2), the complex adopted an elongated shape in good agreement with that found in the X-ray structure (*11*). Finally, we determined the hydration parameter (δ_{IV}) using the intrinsic viscosity relation (see Experimental Procedures). This parameter corresponds to the water molecules bound to the protein as well as to the water molecules dragged by the diffusion of the protein and/or influenced by being in the vicinity of the protein. The isolated CaM and AC displayed hydration of 1 ± 0.1 and 1.5 ± 0.1 g/g, respectively. Interestingly, the hydration decreased markedly to 0.7 ± 0.1 g/g upon complex formation (Table 2). These data indicate that both AC and CaM underwent dehydration upon interaction.

DISCUSSION

In this report, we have characterized the conformational and hydrodynamic changes of the CyaA catalytic domain (AC) triggered by CaM binding in an attempt to obtain biophysical insights into the molecular mechanisms underlying the activation of the AC enzymatic activity.

The secondary and tertiary structure changes of the polypeptides were first characterized by CD and NMR spectroscopies. We showed that the secondary structure of AC is an α/β mixture, without large disordered regions. A prominent finding from CD experiments was that only minor modifications of the secondary structure content of the AC and CaM polypeptides occurred upon their association. Nevertheless, comparison of far-UV CD spectra indicated that association of CaM with AC triggered a small but detectable increment of the overall α-helical structure content of these proteins. We calculated that ~4% of total secondary structure, corresponding to ~20 residues of a total of 534, changed from random coil conformations to α-helical structures upon complex formation. Although the polypeptide region(s) involved in this transition cannot be formally localized, we hypothesized that this structural change occurred in part within the H helix of AC [according to the nomenclature of Guo et al. (*11*); see Figure 7], which constitutes the main CaM-binding site. In agreement with this hypothesis, far-UV CD spectroscopy indicated that a synthetic peptide, $P_{233-254}$, corresponding to the H helix (from residue L233 to G254), adopted random coil conformations in the absence of CaM but acquired helical structures upon binding to CaM, as it has been observed for many other CaM-binding peptides derived from different CaM targets.

Near-UV CD and fluorescence spectroscopy analysis confirmed that whereas in free peptide $P_{233-254}$, tryptophan 242 (W242) was exposed to solvent and highly mobile, it became constrained upon CaM binding, as revealed by the dichroic signal increase at 295 nm and a large blue shift in intrinsic fluorescence. Interestingly, very similar changes in near-UV CD and fluorescence signals (not shown and ref *41* for fluorescence data) were observed with the AC domain as it bound CaM, suggesting that the CaM-induced local structural rearrangement may be similar in both cases. These data are in good agreement with previous results (*42*, *43*), which used time-resolved fluorescence spectroscopy to probe the dynamics of W242. These authors reported that the AC region surrounding this residue was highly dynamic showing nanosecond flexibility in the CaM-free form, and that binding of the activator greatly decreased the local dynamics. It is noteworthy that in anthrax EF, the equivalent H helix is also partly disordered in the CaM-free structure.

Altogether, our data are consistent with a model in which the region around W242 may preferentially adopt an extended conformation in the absence of CaM with the tryptophan being highly mobile and solvent-exposed. Upon association with CaM, this segment would be stabilized in a helical conformation (H helix) and the W242 would become immobilized in a hydrophobic pocket of $CaM_{C\text{-}ter}$ as seen in the crystal structure (*11*).

While CaM binding elicited only minor changes in the secondary and tertiary structure of AC, it had much more pronounced effect on the hydrodynamic properties of the AC protein. Using analytical ultracentrifugation and size exclusion chromatography (SEC) combined with static light scattering and viscosity measurements, we showed that the isolated AC domain was monomeric under native conditions and adopted a globular conformation with a rather high hydration. Upon formation of the complex, the hydration δ_{IV} decreased significantly and the shape became much more elongated with an axial ratio of ~2.7. This latter value is in good agreement with the one

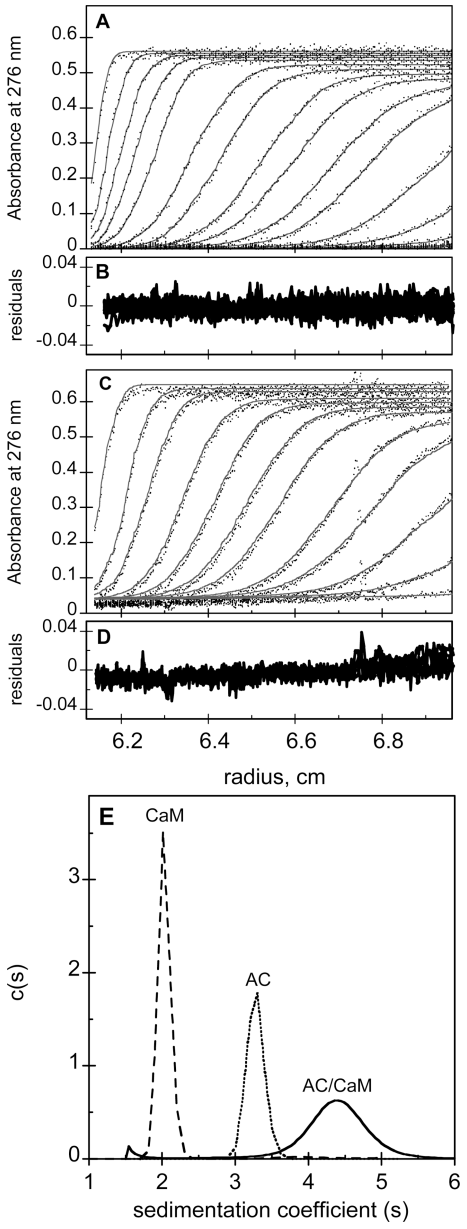

FIGURE 6: Analytical ultracentrifugation analysis of AC, CaM, and the AC−CaM complex (17 μM in buffer A). Experimental data (dots) obtained at 276 nm during AC (A) and AC−CaM (C) sedimentation velocity experiments were fitted with the Lamm equation (lines), and the distribution of the residual values is shown in panels B and D, respectively. (E) Sedimentation coefficient distribution of AC (···), CaM (---), and the AC−CaM complex (—) deduced from the fitted curves. Experimental conditions: buffer A with 0.2 mM $CaCl_2$ at 25 °C.

computed from the crystal structure of the AC−$CaM_{C\text{-}ter}$ complex, although in this complex the N-terminal half of CaM ($CaM_{N\text{-}ter}$) is absent.

The hydrodynamic properties of AC have also been explored by Gallay et al. (*43*), on the basis of fluorescence anisotropy decay measurements. They showed that the average Brownian rotational correlation times of AC differed significantly as a function of the fluorescent probes examined (either AC tryptophans, a fluorescent ATP analogue, or a covalently attached acrylodan probe). It was suggested that AC in the absence of CaM may adopt an elongated shape (with an axial ratio of ~1.9) that would become more elongated (axial ratio of 2.4) upon CaM binding. Although our results agree with a CaM-induced elongation of the

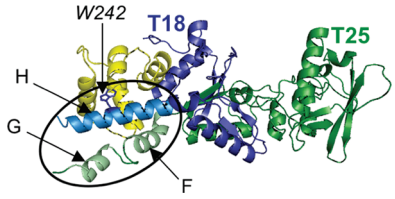

FIGURE 7: Three-dimensional structure of AC complexed with the C-terminal domain of CaM. The picture is drawn from PDB entry 1YRU (*11*) to highlight the positioning of the helical tip made of F, G, and H helices. $CaM_{C\text{-}ter}$ is colored yellow, whereas the T25 and T18 AC regions are colored green and blue, respectively. The side chain of AC W242, buried in a hydrophobic pocket of CaM, is colored dark blue.

AC molecule, they are at variance regarding the overall shape of the free AC protein, as we found that AC is rather globular in the absence of CaM. Indeed, the viscosity increment of 2.5 calculated for the free AC in solution corresponds to an a/b axial ratio of 1 ($a = b = R_H$), which is indicative of a nearly spherical conformation. The discrepancy regarding the shape of AC may be related to the different experimental approaches used. Indeed, Gallay and colleagues estimated the dynamics of the whole protein by extrapolation of time-resolved fluorescence anisotropy decays of small probes, yet these values depend not only on the overall protein hydrodynamics but also on the probe flexibility. In this study, the hydrodynamic properties of the proteins were characterized by AUC, SEC-TDA, and DLS. These latter biophysical approaches provide hydrodynamic parameters based directly on the behavior of the corresponding molecules and therefore should be considered as more reliable.

The observation that AC adopts a globular conformation in the absence of CaM has direct implications for the possible conformational changes elicited by CaM binding. In the crystal structure, the AC−CaM complex appears as an extended rod ~10 nm in length and ~4 nm in diameter (Figure 7). One tip of this rod is made by the H helix, bound to $CaM_{C\text{-}ter}$, together with the two preceding short helices F and G at the C-terminus of the T25 region. The H helix is aligned with the main axis of the rod and points out, contributing to approximately one-third of the AC overall length. On the basis of our data, we can hypothesize that in the absence of CaM, this helical tip as well as the T18 region (dark blue in Figure 7) fold back onto the core of the T25 region of the catalytic domain (Figure 7). This structural organization may be associated with a partially unfolded H helix as suggested from our CD data discussed above. Such a reorientation of the F, G, and H helices and the rest of the T18 region relative to the catalytic core would significantly shorten the long axis of the molecule, hence giving rise to a much more globular conformation in agreement with our hydrodynamic measurements.

It is interesting to note that the corresponding F, G, and H helices of the anthrax EF toxin, the so-called switch A according to Drum et al. (*15*), also undergo a significant conformational rearrangement between the CaM-free and CaM-bound forms, in a manner fairly similar to the one suggested above for AC. In the CaM-bound form, the H helix of *B. anthracis* EF is also roughly aligned with the main axis of the catalytic core (domains C_A and C_B). In the absence of CaM, the H helix is rotated ~50° relative to the main axis to dock onto the C-terminal helical domain, which is the main CaM-binding site of EF (*15*). It is noteworthy that, as in AC an equivalent C-terminal helical domain is absent, the corresponding H helix would have enough space to rotate up to

90° in the CaM-free conformation and dock onto the side of the C_A domain of the catalytic core.

CaM establishes numerous contacts with the T18 moiety of AC, predominantly with the H helix, but also with C-terminal helices J and J′ ["C-tail" according to Guo et al. (*11*)] and thus may directly contribute to lock the T18 region into a stable and active conformation. In the absence of this activator, the T18 polypeptide might be more flexible and hydrated as suggested by our results. These data actually support the view that the secondary structure content of the T18 fragment is not dramatically altered in the CaM-free AC, as evidenced from the global conservation of the secondary structures (CD), the absence of large disordered regions (NMR), and the overall globular shape (hydrodynamic studies) of the molecule. The reorganization of the helical tip (i.e., F, G, and H helices) in the CaM-free AC may be accompanied by some repositioning of the T18 polypeptide, thus disrupting the local topological arrangement of the CR3 region of the catalytic site and consequently altering the enzymatic activity. A higher dynamics of the whole T18 polypeptide and especially of the CR3 region may also contribute to the dramatic reduction of the catalytic efficiency of the AC enzyme in the absence of the activator. This model could explain that AC retains a weak but detectable enzymatic activity in the absence of CaM, at variance with EF, which appears to be locked in a totally inactive state in the absence of the activator.

In conclusion, the results presented here shed new light on the molecular shape of the catalytic domain of CyaA and on the structural rearrangements elicited by CaM binding. Our data indicate that although CaM binding triggers only limited modifications in the secondary and tertiary structures of AC, it induces a significant elongation, dehydration, and compaction of the protein. We propose that these conformational changes stabilize the enzymatically active form of AC by remodeling the catalytic site, in a process very similar to that found in EF. This would suggest that the *B. pertussis* and *B. anthracis* adenylate cyclase toxins share a common mechanism of activation, although their primary sequence and structural basis for interacting with their common CaM activator have largely diverged.

ACKNOWLEDGMENT

We thank Agnès Ullmann for critical reading of the manuscript and Muriel Delepierre for fruitful discussions and for providing access to the 600 MHz spectrometer. We thank Jacques D'Alayer for N-terminal sequencing and mass spectrometry and the Plate-forme de Biophysique des Macromolécules et de leurs Interactions for providing access to the CD, DLS, TDA, and AUC instruments.

REFERENCES

1. Ladant, D., and Ullmann, A. (1999) *Bordetella pertussis* adenylate cyclase: A toxin with multiple talents. *Trends Microbiol. 7*, 172–176.
2. Vojtova, J., Kamanova, J., and Sebo, P. (2006) *Bordetella* adenylate cyclase toxin: A swift saboteur of host defense. *Curr. Opin. Microbiol. 9*, 69–75.
3. Harvill, E. T., Cotter, P. A., Yuk, M. H., and Miller, J. F. (1999) Probing the function of *Bordetella bronchiseptica* adenylate cyclase toxin by manipulating host immunity. *Infect. Immun. 67*, 1493–1500.
4. Perkins, D. J., Gray, M. C., Hewlett, E. L., and Vogel, S. N. (2007) *Bordetella pertussis* adenylate cyclase toxin (ACT) induces cyclooxygenase-2 (COX-2) in murine macrophages and is facilitated by ACT interaction with CD11b/CD18 (Mac-1). *Mol. Microbiol. 66*, 1003–1015.
5. Cheung, G. Y., Dickinson, P., Sing, G., Craigon, M., Ghazal, P., Parton, R., and Coote, J. G. (2008) Transcriptional responses of murine macrophages to the adenylate cyclase toxin of *Bordetella pertussis*. *Microb. Pathog. 44*, 61–70.
6. Rose, T., Sebo, P., Bellalou, J., and Ladant, D. (1995) Interaction of calcium with *Bordetella pertussis* adenylate cyclase toxin. Characterization of multiple calcium-binding sites and calcium-induced conformational changes. *J. Biol. Chem. 270*, 26370–26376.
7. Bauche, C., Chenal, A., Knapp, O., Bodenreider, C., Benz, R., Chaffotte, A., and Ladant, D. (2006) Structural and functional characterization of an essential RTX subdomain of *Bordetella pertussis* adenylate cyclase toxin. *J. Biol. Chem. 281*, 16914–16926.
8. Chenal, A., Guijarro, J. I., Raynal, B., Delepierre, M., and Ladant, D. (2009) RTX calcium binding motifs are intrinsically disordered in the absence of calcium: Implication for protein secretion. *J. Biol. Chem. 284*, 1781–1789.
9. Danchin, A. (1993) Phylogeny of adenylyl cyclases. *Adv. Second Messenger Phosphoprotein Res. 27*, 109–162.
10. Shen, Y., Zhukovskaya, N. L., Guo, Q., Florian, J., and Tang, W. J. (2005) Calcium-independent calmodulin binding and two-metal-ion catalytic mechanism of anthrax edema factor. *EMBO J. 24*, 929–941.
11. Guo, Q., Shen, Y., Lee, Y. S., Gibbs, C. S., Mrksich, M., and Tang, W. J. (2005) Structural basis for the interaction of *Bordetella pertussis* adenylyl cyclase toxin with calmodulin. *EMBO J. 24*, 3190–3201.
12. Glaser, P., Elmaoglou-Lazaridou, A., Krin, E., Ladant, D., Barzu, O., and Danchin, A. (1989) Identification of residues essential for catalysis and binding of calmodulin in *Bordetella pertussis* adenylate cyclase by site-directed mutagenesis. *EMBO J. 8*, 967–972.
13. Glaser, P., Munier, H., Gilles, A. M., Krin, E., Porumb, T., Barzu, O., Sarfati, R., Pellecuer, C., and Danchin, A. (1991) Functional consequences of single amino acid substitutions in calmodulin-activated adenylate cyclase of *Bordetella pertussis*. *EMBO J. 10*, 1683–1688.
14. Munier, H., Bouhss, A., Krin, E., Danchin, A., Gilles, A. M., Glaser, P., and Barzu, O. (1992) The role of histidine 63 in the catalytic mechanism of *Bordetella pertussis* adenylate cyclase. *J. Biol. Chem. 267*, 9816–9820.
15. Drum, C. L., Yan, S. Z., Bard, J., Shen, Y. Q., Lu, D., Soelaiman, S., Grabarek, Z., Bohm, A., and Tang, W. J. (2002) Structural basis for the activation of anthrax adenylyl cyclase exotoxin by calmodulin. *Nature 415*, 396–402.
16. Ladant, D. (1988) Interaction of *Bordetella pertussis* adenylate cyclase with calmodulin. Identification of two separated calmodulin-binding domains. *J. Biol. Chem. 263*, 2612–2618.
17. Ladant, D., Michelson, S., Sarfati, R., Gilles, A. M., Predeleanu, R., and Barzu, O. (1989) Characterization of the calmodulin-binding and of the catalytic domains of *Bordetella pertussis* adenylate cyclase. *J. Biol. Chem. 264*, 4015–4020.
18. Munier, H., Bouhss, A., Gilles, A. M., Krin, E., Glaser, P., Danchin, A., and Barzu, O. (1993) Structural flexibility of the calmodulin-binding locus in *Bordetella pertussis* adenylate cyclase. Reconstitution of catalytically active species from fragments or inactive forms of the enzyme. *Eur. J. Biochem. 217*, 581–586.
19. Bouhss, A., Krin, E., Munier, H., Gilles, A. M., Danchin, A., Glaser, P., and Barzu, O. (1993) Cooperative phenomena in binding and activation of *Bordetella pertussis* adenylate cyclase by calmodulin. *J. Biol. Chem. 268*, 1690–1694.
20. Guo, Q., Jureller, J. E., Warren, J. T., Solomaha, E., Florian, J., and Tang, W. J. (2008) Protein-protein docking and analysis reveal that two homologous bacterial adenylyl cyclase toxins interact with calmodulin differently. *J. Biol. Chem. 283*, 23836–23845.
21. Vougier, S., Mary, J., Dautin, N., Vinh, J., Friguet, B., and Ladant, D. (2004) Essential role of methionine residues in calmodulin binding to *Bordetella pertussis* adenylate cyclase, as probed by selective oxidation and repair by the peptide methionine sulfoxide reductases. *J. Biol. Chem. 279*, 30210–30218.
22. Lees, J. G., Miles, A. J., Wien, F., and Wallace, B. A. (2006) A reference database for circular dichroism spectroscopy covering fold and secondary structure space. *Bioinformatics 22*, 1955–1962.
23. Lobley, A., Whitmore, L., and Wallace, B. A. (2002) DICHROWEB: An interactive website for the analysis of protein secondary structure from circular dichroism spectra. *Bioinformatics 18*, 211–212.
24. Whitmore, L., and Wallace, B. A. (2004) DICHROWEB, an online server for protein secondary structure analyses from circular dichroism spectroscopic data. *Nucleic Acids Res. 32*, W668–W673.
25. Compton, L. A., and Johnson, W. C., Jr. (1986) Analysis of protein circular dichroism spectra for secondary structure using a simple matrix multiplication. *Anal. Biochem. 155*, 155–167.
26. Sreerama, N., and Woody, R. W. (2000) Estimation of protein secondary structure from circular dichroism spectra: Comparison of

CONTIN, SELCON, and CDSSTR methods with an expanded reference set. *Anal. Biochem. 287*, 252–260.
27. Manavalan, P., and Johnson, W. C., Jr. (1987) Variable selection method improves the prediction of protein secondary structure from circular dichroism spectra. *Anal. Biochem. 167*, 76–85.
28. Cao, W., and Demeler, B. (2005) Modeling analytical ultracentrifugation experiments with an adaptive space-time finite element solution of the Lamm equation. *Biophys. J. 89*, 1589–1602.
29. Schuck, P. (2000) Size-distribution analysis of macromolecules by sedimentation velocity ultracentrifugation and Lamm equation modeling. *Biophys. J. 78*, 1606–1619.
30. Schuck, P. (2003) On the analysis of protein self-association by sedimentation velocity analytical ultracentrifugation. *Anal. Biochem. 320*, 104–124.
31. Bourdeau, R. W., Malito, E., Chenal, A., Bishop, B. L., Musch, M. W., Villereal, M. L., Chang, E. B., Mosser, E. M., Rest, R. F., and Tang, W. J. (2009) Cellular Functions and X-ray Structure of Anthrolysin O, a Cholesterol-dependent Cytolysin Secreted by *Bacillus anthracis*. *J. Biol. Chem. 284*, 14645–14656.
32. Barbato, G., Ikura, M., Kay, L. E., Pastor, R. W., and Bax, A. (1992) Backbone dynamics of calmodulin studied by ^{15}N relaxation using inverse detected two-dimensional NMR spectroscopy: The central helix is flexible. *Biochemistry 31*, 5269–5278.
33. Sreerama, N., Manning, M. C., Powers, M. E., Zhang, J. X., Goldenberg, D. P., and Woody, R. W. (1999) Tyrosine, phenylalanine, and disulfide contributions to the circular dichroism of proteins: Circular dichroism spectra of wild-type and mutant bovine pancreatic trypsin inhibitor. *Biochemistry 38*, 10814–10822.
34. Freskgard, P. O., Martensson, L. G., Jonasson, P., Jonsson, B. H., and Carlsson, U. (1994) Assignment of the contribution of the tryptophan residues to the circular dichroism spectrum of human carbonic anhydrase II. *Biochemistry 33*, 14281–14288.
35. Tavallaie, M., Chenal, A., Gillet, D., Pereira, Y., Manich, M., Gibert, M., Raffestin, S., Popoff, M. R., and Marvaud, J. C. (2004) Interaction between the two subdomains of the C-terminal part of the botulinum neurotoxin A is essential for the generation of protective antibodies. *FEBS Lett. 572*, 299–306.
36. Fasman, G. D., Ed. (1996) Circular Dichroism and the Conformational Analysis of Biomolecules, Plenum Press, New York.
37. Ikura, M., Clore, G. M., Gronenborn, A. M., Zhu, G., Klee, C. B., and Bax, A. (1992) Solution structure of a calmodulin-target peptide complex by multidimensional NMR. *Science 256*, 632–638.
38. Meador, W. E., Means, A. R., and Quiocho, F. A. (1992) Target enzyme recognition by calmodulin: 2.4 Å structure of a calmodulin-peptide complex. *Science 257*, 1251–1255.
39. Meador, W. E., Means, A. R., and Quiocho, F. A. (1993) Modulation of calmodulin plasticity in molecular recognition on the basis of X-ray structures. *Science 262*, 1718–1721.
40. Harding, S. E., and Colfen, H. (1995) Inversion formulae for ellipsoid of revolution macromolecular shape functions. *Anal. Biochem. 228*, 131–142.
41. Gilles, A. M., Munier, H., Rose, T., Glaser, P., Krin, E., Danchin, A., Pellecuer, C., and Barzu, O. (1990) Intrinsic fluorescence of a truncated *Bordetella pertussis* adenylate cyclase expressed in *Escherichia coli*. *Biochemistry 29*, 8126–8130.
42. Bouhss, A., Vincent, M., Munier, H., Gilles, A. M., Takahashi, M., Barzu, O., Danchin, A., and Gallay, J. (1996) Conformational transitions within the calmodulin-binding site of *Bordetella pertussis* adenylate cyclase studied by time-resolved fluorescence of Trp242 and circular dichroism. *Eur. J. Biochem. 237*, 619–628.
43. Gallay, J., Vincent, M., Li de la Sierra, I. M., Munier-Lehmann, H., Renouard, M., Sakamoto, H., Barzu, O., and Gilles, A. M. (2004) Insight into the activation mechanism of *Bordetella pertussis* adenylate cyclase by calmodulin using fluorescence spectroscopy. *Eur. J. Biochem. 271*, 821–833.